Liquefaction Potential Analysis Along Coastal Area of Bengkulu Province due to the 2007 M_w 8.6 Bengkulu Earthquake

Lindung Zalbuin Mase

Department of Civil Engineering. Faculty of Engineering, University of Bengkulu, WR Supratman Rd, Kandang Limun, Muara Bangkahulu, Bengkulu, 38371, Indonesia
E-mail: lmase@unib.ac.id

Abstract. This paper presents a seismic response analysis study of liquefiable sites along the northern parts of the coastal area of Bengkulu Province that underwent liquefaction phenomena during the strong earthquake (8.6 M_w) on 12 September 2007. Several investigation tests, including the standard penetration test (SPT) and the soil shear wave velocity test, were conducted at 8 locations. The data were used to simulate the seismic response in order to investigate soil behaviors during the earthquake. In addition, the excess pore water pressure ratio obtained from the analysis was compared with the prediction value calculated from empirical data. The results show that liquefaction can occur at shallow depth layers dominated by loose sand. The results also confirm field evidence collected during the earthquake that was reported in several previous studies. The excess pore water pressure ratio was in good agreement with the predicted value from the empirical approach.

Keywords: *Bengkulu; coastal area; liquefaction; sandy soil; strong earthquake.*

1 Introduction

On September 12, 2007, an earthquake with a magnitude of 8.6 M_w occurred in the Indian Ocean (Figure 1) and resulted in huge damage in Bengkulu Province [1,2]. This earthquake also triggered the unique phenomenon known as liquefaction, especially along the coastal areas of the province [3]. To learn from the earthquake event in 2007, an intensive liquefaction study was performed.

Several local researchers have performed preliminary studies to estimate the liquefaction potential in Bengkulu Province [3-7]. In general, the previous studies analyzed the liquefaction severity based on an empirical approach, as proposed by Seed and Idriss [8] and Idriss and Boulanger [9]. These previous studies reached the conclusion that the coastal areas in Bengkulu could undergo liquefaction at shallow depth. However, a description of liquefiable soil behavior under earthquake loading was not achieved in the previous studies.

Received April 20th, 2017, Revised October 18th, 2017, Accepted for publication December 14th, 2017.
 ISSN: 2337-5779, DOI: 10.5614/j.eng.technol.sci.2017.49.6.2

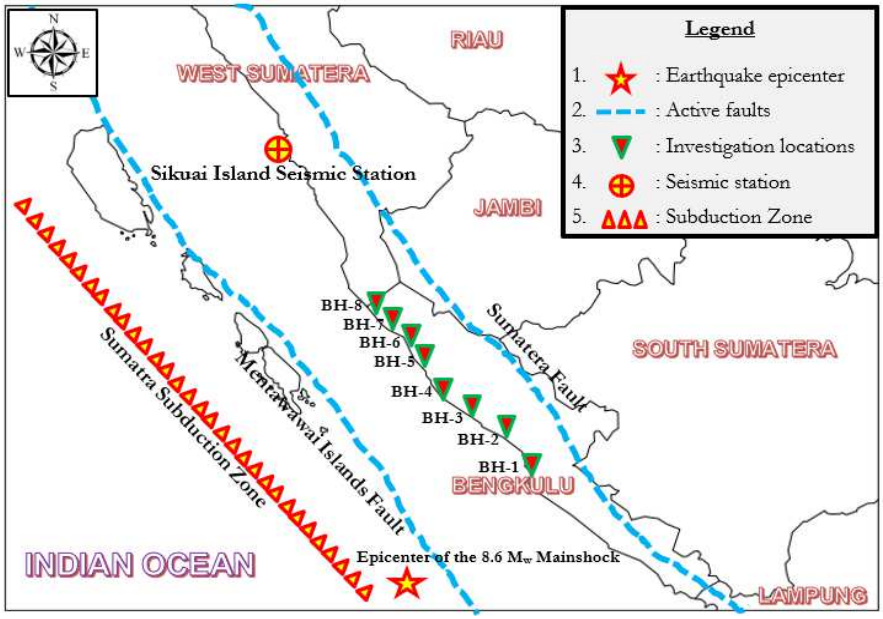

Figure 1 Location of the earthquake epicenter and site investigation sites.

This paper presents a site response analysis of a number of liquefaction sites spread along the coastal area of Bengkulu City. Eight site investigation tests, including the standard penetration test (SPT) and the shear wave velocity test (V_S), were performed. Locations in Bengkulu City, North Bengkulu, Central Bengkulu, and Mukomuko regency underwent liquefaction in September 2007, as reported by the Earthquake Engineering Research Institute (EERI) [10]. Soil behaviors including excess pore pressure ratio (r_u) time history, hysteresis loop, and effective stress (σ_v') reduction are presented here. In addition, a comparison of r_u values obtained from the analysis with the predicted values based on empirical data was performed. Overall, this study was expected to provide a better understanding of the liquefaction phenomenon that occurred in Bengkulu Province and raise awareness to the impact of earthquakes among people living in the coastal areas of Bengkulu Province.

2 Theory

2.1 Non-linear Site Response Analysis of Liquefiable Layer

The cyclic stress-strain behavior under dynamic load in saturated sandy soil is a complex phenomenon, especially in terms of pore pressure generation. Ishihara, *et al*. [11] introduced the phase transformation (PT) of sand during cyclic loading to explain this complex behavior. A detailed phase-by-phase

explanation during cyclic loading is presented in Figure 2. In cyclic loading, there are two kinds of loading, i.e. compression and extension; therefore, in Figure 2, there are two PT lines, i.e. one for compression loading and another one for extension loading.

Once the compression loading is applied, the cyclic loading moves the initial value of effective stress (Phase A) to the left side, which indicates there is a transformation of soil behavior from contraction to dilation (Phase B). Furthermore, there is the increment of soil stiffness, which is followed by excess pore water pressure in Phase C. When the loading is reversed back, the extension loading makes the effective confining pressure decrease, as seen in Phase D, and the soil behaves as a contracted material with the reduction of pore pressure accumulation. Once the compression loading is applied again, the effective stress path moves to the right in Phase E and passes the compression PT line as seen in Phase F. This condition is followed by an increment of soil stiffness in Phase G.

The accumulated pore pressure decreases (Phase H) and may reach the PT line for extension loading in Phase I, which is followed by the increase of soil stiffness in Phase J. In the first cycle (Phase A to J) there is not only an accumulation of pore pressure but also a decrease of accumulation of pore pressure. In the second cycle, the effective stress path will show similar phases as in the first cycle. From the illustration in Figure 2, the cyclic phenomenon in sandy soils is very complex and non-linear; therefore, it is necessary to use sophisticated soil modeling to describe it. The complex phenomena previously illustrated suggest consideration of the cyclic behavior in terms of seismic response analysis.

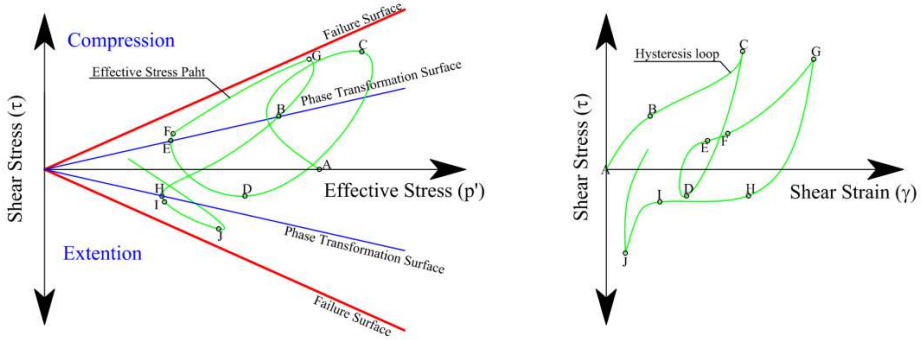

Figure 2 Effective stress path and shear strain-shear stress of under dynamic load [redrawn from Elgamal *et al*. [12]] (p' is mean effective stress), τ is shear stress, γ is shear strain, PT is the phase transformation surface).

Iai, *et al*. [13] proposed a non-linear effective stress model composed of two main models. The first model is a multi-spring element model, as presented in Figure 3(a), with the hyperbolic non-linear model defined in strain space, which considers the rotation of the principle stress axis direction. This effect plays a role in the cyclic behavior of anisotropy-consolidated sand [15]. The multi-spring element model is generated with the shearing section in a direction in which the hyperbola model works. This model can also simulate the hysteresis loop.

The second model, as presented in Figure 3(b), is an effective stress model, which applies the plastic shear work and stress. This model simulates the excess pore water pressure as a function of cumulative shear work. Moreover, the effect of dilatancy is considered in cyclic mobility behavior of the liquefaction front stated in the effective stress space. This model can also simulate rapid or gradual increments in cyclic strain amplitude under undrained cyclic loading.

2.2 Empirical Analysis of Liquefaction

In empirical analysis, the severity of liquefaction is normally noted as P_L (probability of liquefaction) and FS_L (liquefaction factor of safety). P_L can be estimated as done by Liao *et al*. [16] using Eqs. (1) and (2).

$$P_L = \frac{1}{1+\exp[-(\beta_0 + \beta_1 \ln(CSR) + \beta_2 (N_1)_{60})]} \tag{1}$$

$$CSR = 0.65 \frac{\sigma_v . a_{\max} . r_d}{\sigma_v^{'} . g} \tag{2}$$

where P_L is probability of liquefaction, CSR is the cyclic resistance ratio, $(N_1)_{60}$ is the corrected SPT (blows/ft), β_0, β_1, β_2 are constant values, σ_v is total stress (kPa), σ_v' is effective stress (kPa), a_{max} is maximum PGA (g), g is gravity acceleration (9.81 m/s^2), and r_d is the depth reduction factor (1-0.015z, (z is analyzed depth)).

The back analysis employing the P_L model was used to estimate FS_L by using Chen and Juang's [17] model, which is expressed in Eq. (3). The results can also be compared with data from an empirical approach, especially to predict r_u, using Yegian and Vittel's [19] model, as shown in Eq. (4),

$$P_L = \frac{1}{1+\left(\frac{FS_L}{1.25}\right)^{3.76}} \tag{3}$$

$$r_u = \frac{2}{\pi}\arcsin\left(\frac{1}{FS_L}\right)^{\frac{1}{2\alpha\beta}} \quad (4)$$

where α and β are constants of 0.7 and 0.19 respectively.

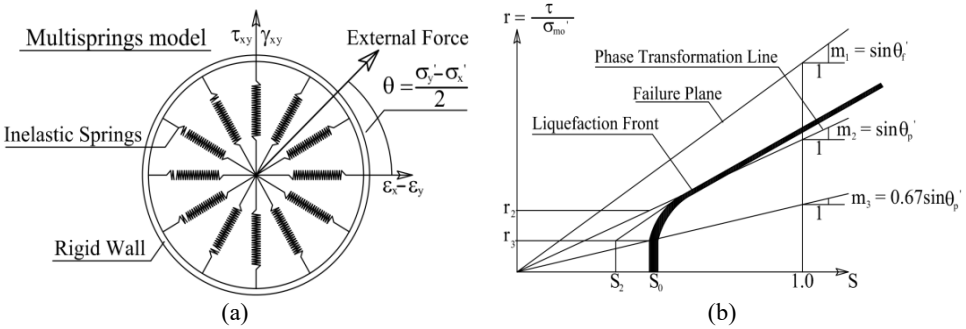

Figure 3 Effective stress model of Iai, *et al*. [13]. (a) Schematic of multi-spring element model [redrawn from Sawada, *et al*. [14]] (τ_{xy} and γ_{xy} are shear stress and shear strain, respectively, θ is the angle between external force and strain (ε_x-ε_y) horizontal direction); (b) schematic of liquefaction front, state variable (S), and τ ratio (r) [redrawn from Iai, *et al*. [13]] (m_1 is the inclination of failure, which equals sin θ_f (friction angle of failure), m_2 is the inclination of phase transformation, which equals sin θ_p (friction angle of phase transformation line), and m_3 is the inclination between the horizontal axis of the state variable and the phase transformation line, which equals 0.67sinθ_p), τ is shear stress, and σ_{mo}' is initial σ_v').

3 Data and Method

3.1 Study Area and Site Investigation Result

The location of the study area is presented in Figure 1. The investigation sites are spread along the coast of Bengkulu. The sites are noted as BH-1 to BH-6, representing Pantai Panjang (BH-1), Lais (BH-2), Ketahun (BH-3), Air Muring (BH-4), Air Buluh (BH-5), Air Hitam (BH-6), Pasar Bantal (BH-7), and Mukomuko (BH-8). The results of the site investigations are presented in Figure 4. Based on the site investigation results, the geological condition of the coastal areas of Bengkulu Province is dominated by sandy soils, with ground water level near ground surface (about 0.3 to 0.5 m). Loose sand (SP) layers are found at shallow depth (0 to 7.5 m) with an $(N_1)_{60}$ average of 1-8 blows/ft and FC (fine contents) of 5%. Silty sand (SM) layers are generally found at 7.5 to 27 m depth, with an $(N_1)_{60}$ average of 8 to 35 blows/ft and FC of 12%.

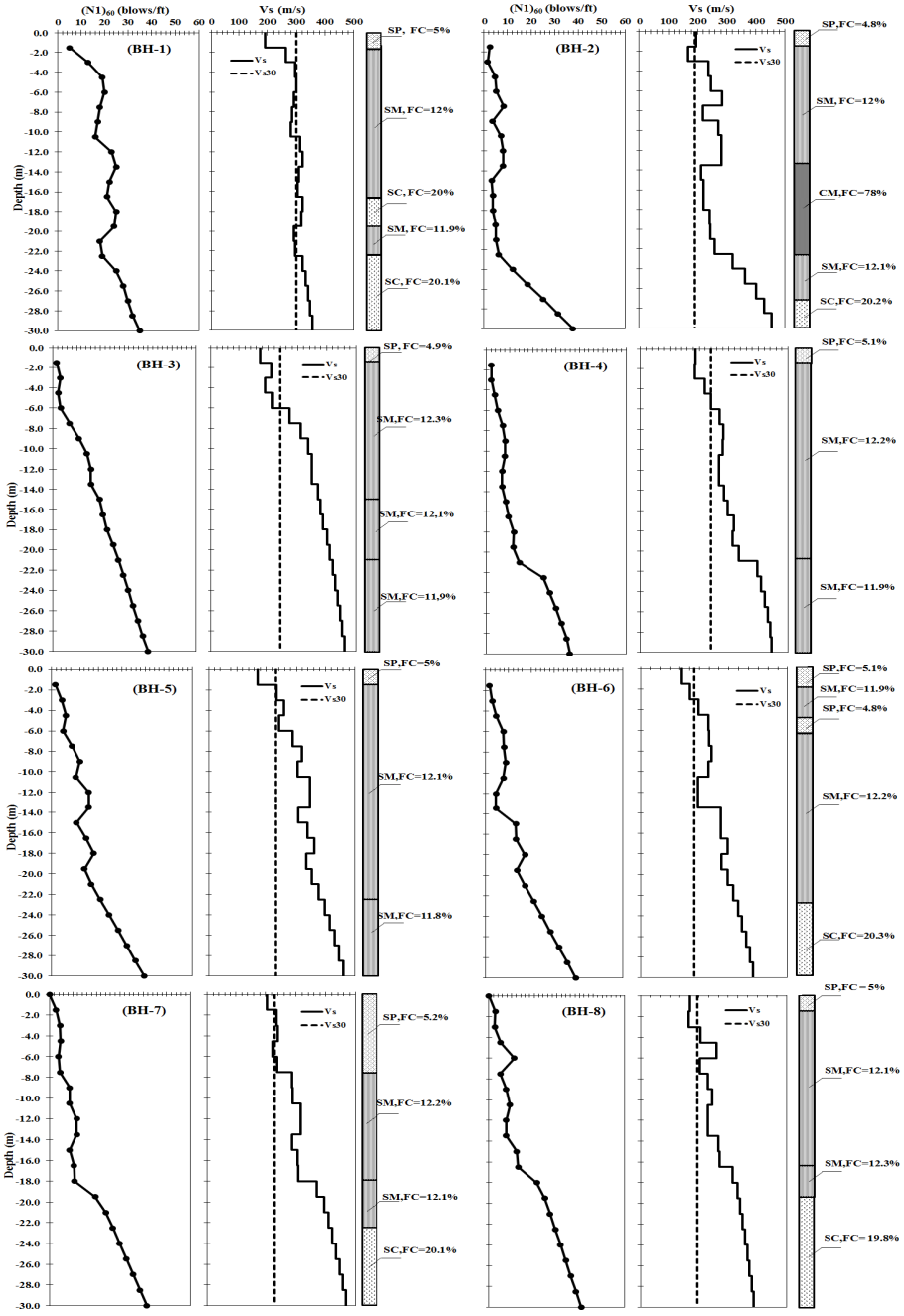

Figure 4 Site investigation results.

Clayey sand (SC) layers are found at 27 to 30 m depth, with an $(N_1)_{60}$ average of 34 to 43 blows/ft and FC of 20%. According to the National Earthquake Hazard Reduction Program (NEHRP) [19], the study area can be categorized as stiff soil with an average of the first 30-m shear wave velocity (V_{S30}) of about 190-300 m/s.

3.2 Ground Motion of the 8.6 M_w Earthquake in September 2007

The ground motion of the September 2007 earthquake (Figure 5) was recorded at only one station, i.e. Sikuai Island Seismic Station, which is very far removed from the study area (393 km away from the epicenter). The earthquake ground motion was obtained from the Centre of Earthquake Strong Motion Database (CESMD) [20]. For the other locations, there were no data showing the ground motion (because there are no seismic stations in the study area). However, the recorded ground motion in Sikuai Island can generally give an appropriate interpretation of the ground motion parameters (Table 1) to describe the earthquake.

In Table 1, the maximum value of peak ground acceleration (PGA_{max}), the maximum peak ground velocity maximum (PGV_{max}), and the maximum value of peak ground displacement maximum (PGD_{max}) were 0.0408 g, 4.19144 cm/sec, and 10.2367 cm, respectively. These maximum values occurred at 61.16 sec, 61.11 sec, and 71.14 sec, respectively.

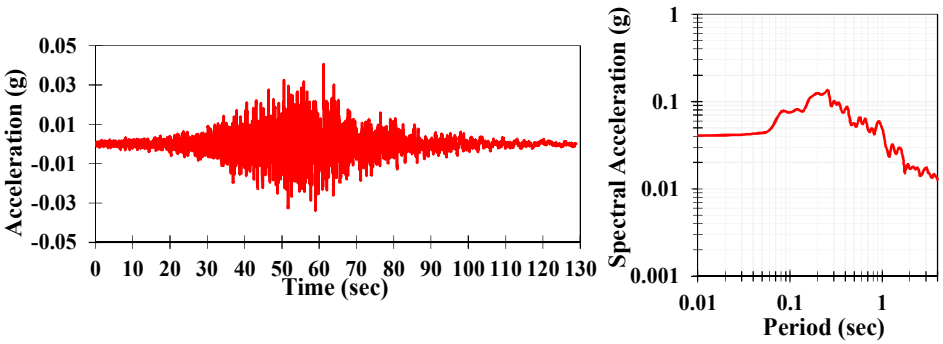

Figure 5 Recorded ground motion measured in Sikuai Island [20].

The ratio of PGV_{max} and PGA_{max} was 0.1047 sec, which implies a ground period (T_g) of 0.658 sec ($T_g=2\pi$ (PGV_{max}/ PGA_{max})). Housner intensity of the ground motion was 13.457 cm with a maximum specific energy density (energy flux) of 129.3712 cm^2/sec (Figure 6). The significant duration of the recorded ground motion (duration between 5% and 95% of arias intensity) was 44.935 sec, as detailed in Figure 6.

Table 1 Summary of ground motion parameters.

Parameter	Values	Units
Maximum acceleration (PGA_{max})	0.0408	g
Time of maximum acceleration	61.1550	sec
Maximum velocity (PGV_{max})	4.1914	cm/sec
Time of maximum velocity	61.1100	sec
Maximum displacement (PGD_{max})	10.2367	cm
Time of maximum displacement	71.1400	sec
PGV_{max} / PGA_{max}	0.1047	sec
Housner intensity	13.4570	cm
Predominant period (T_o)	0.2600	sec
Significant duration	44.935	sec

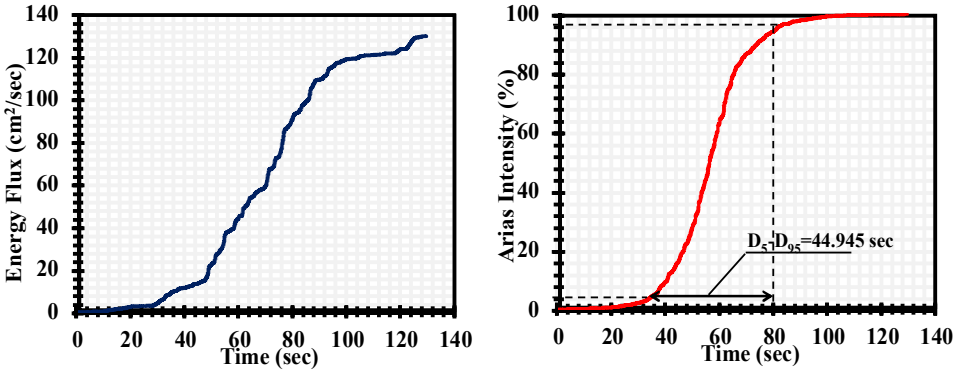

Figure 6 Energy density and arias intensity of the recorded ground motion.

Since there are no recorded ground motions available for the study area, PGA_{max} (maximum PGA) in the study area had to be predicted using an attenuation model. In this study, the attenuation model of Youngs, *et al*. [21] was used. The ground motion predictions and spectral accelerations of the sites are shown in Figure 7. The predicted PGA_{max} ranged from 0.0892 g to 0.1542 g.

The maximum value of PGA_{max} from the attenuation model was calculated for the BH-1 site and the minimum one was calculated for the BH-8 site. These sites are the closest and the farthest from the epicenter of the earthquake that occurred in September 2007 (Figure 1) respectively. In terms of spectral acceleration, the maximum value consistently occurred at period (T) of 0.3 sec or frequency (f) of 3.3 Hz (simply predicted by $f = 1/T$). Consistent with the maximum PGA_{max}, BH-1 and BH-2 had the maximum and minimum spectral acceleration respectively.

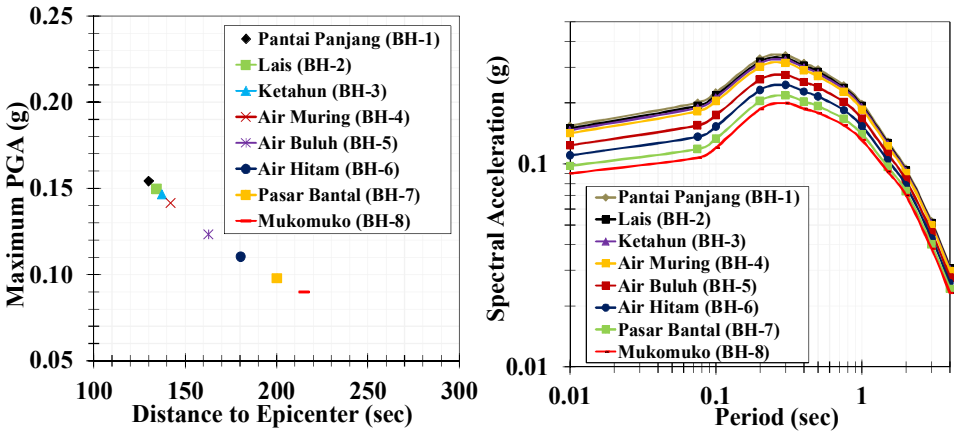

Figure 7 The predictions of maximum PGA and spectral acceleration.

3.3 Method

This study started with site investigations in the coastal areas of Bengkulu Province. SPT data and V_S data were collected and studied to understand the sub-soil conditions in the study area. In addition, the ground motion measured at Sikuai Island Seismic Station was studied to understand the ground motion parameters. All collected data were used to conduct an element simulation to find the liquefaction characteristics of the soil layers using a simplified element simulation method (Morita, *et al.* in [22]). After the characteristics of liquefaction strength were achieved, a one-dimensional site response analysis was conducted. At this stage, the input material, i.e. unit weight (γ_{sat}), FC, SPT, V_S of soil layer, ν (Poisson's ratio), was used. The input motion was applied at the bottom of each borehole. In this study, the spectral accelerations of the sites (calculated based on Youngs, *et al.* [21]) were matched with the spectral accelerations of the recorded ground motion.

The matched spectral accelerations were then derived to generate the input motions for the sites (Figure 8). The results of the simulation, including r_u time history, τ-ε hysteresis loop, and σ_v' path, are presented in the next section. The liquefactions are signed by r_u equal or more than 1. In this paper, only the results of selected layers are presented, which represent different soil types. Another result of the site response analysis, i.e. the amplification factor of each site, is also presented to determine which sites had the highest and the lowest amplification factor. PGA_{max} at ground surface at each site resulted from the site response analysis was used in the empirical analysis of the liquefaction to estimate P_L using the formulation of Liao, *et al.* in [16], which was furthermore used to estimate FS_L using the back-analysis method using Chen and Juang's

[17] formulation. The results of the empirical analysis were plotted with r_u and compared with the values of r_u predicted by Yegian and Vittel in [18].

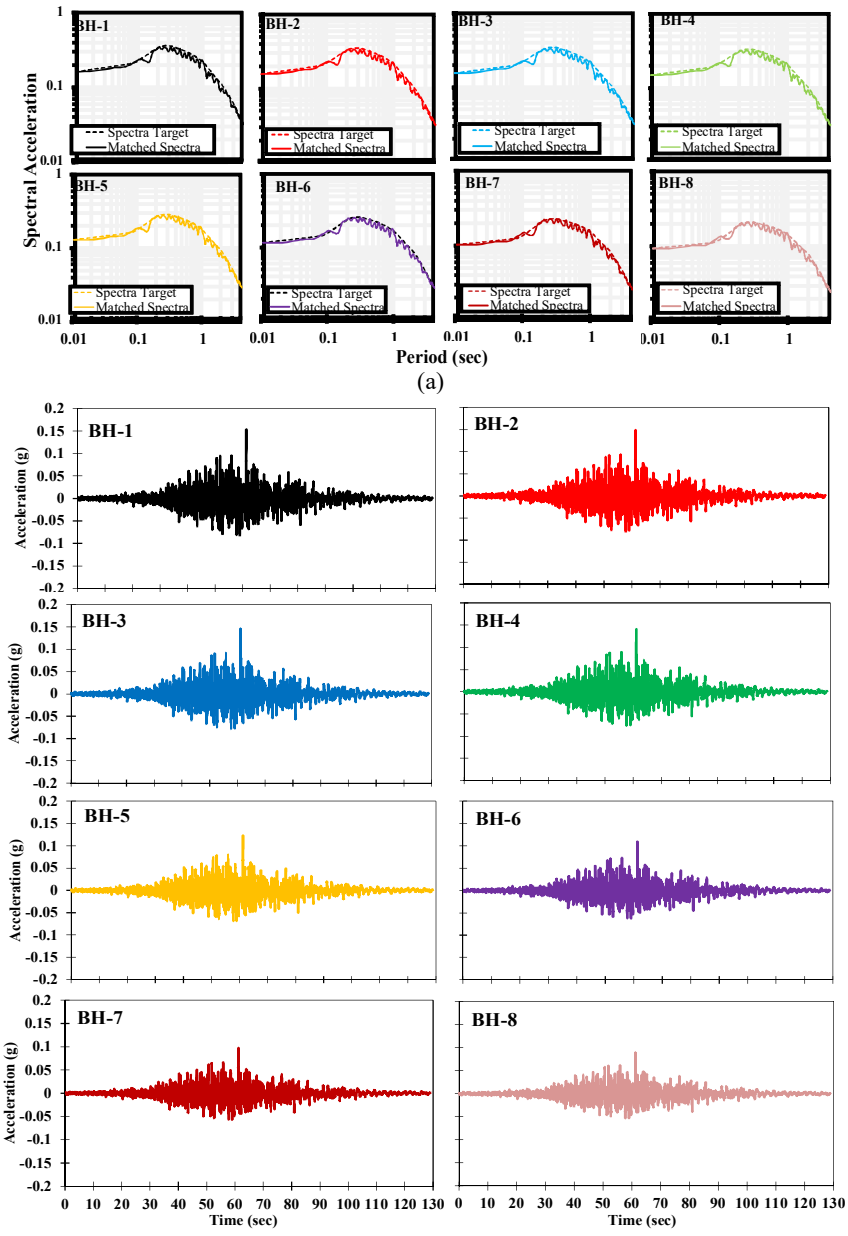

Figure 8 The input motions: (a) spectra acceleration comparison, (b) input motion derived from matched spectra.

4 Result and Discussion

4.1 Liquefaction Resistance Curve

The liquefaction resistance curves of the potentially liquefiable soil layers are shown in Figure 9. The results obtained by simulating the experimental results as the reference or the target liquefaction strength were compared to the investigated layers. The element simulation inputs used in this study were $(N_1)_{60}$, FC, and σ_v'. The subsoil layers located at shallow depth had lower liquefaction strength than the experimental tests, especially SP and SM. These soil layers had low soil resistance ($(N_1)_{60}$ less than 15 blows/ft) and low σ_v'. Based on this result, we could simply predict that liquefaction possibly happens in these soil layers. Overall, soil layer 1 (SP) of BH-2 had the lowest liquefaction resistance, since the liquefaction could happen during a very low cyclic strain, i.e. 0.1 to 0.2. On the other hand, sand layer 3 (SM) of BH-3 had the highest liquefaction strength where liquefaction could occur within a cyclic strain of 20 to 30.

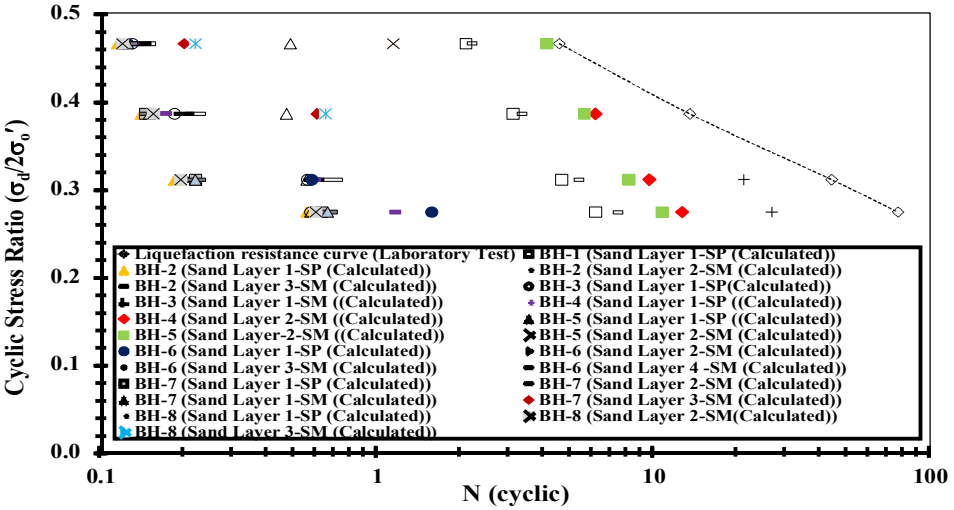

Figure 9 Liquefaction resistance curve of subsoils in the study area.

4.2 Soil Behavior under Input Motion

Examples of soil behavior under the input motion are presented in Figure 10. These examples represent the three soil types that are dominant in the study area, i.e. SP, SM, and SC. Liquefaction possibly occurred in the SP layers at each site, which exist at 0 m to 7.5 m depth. These soil layers had very low $(N_1)_{60}$, FC $\leq$ 5%, and small σ_v' (5.224 to 27.859 kPa). The maximum excess pore pressure ratio ($r_u$max) of the layers ranged from 0.974 to 0.999. The soil

behavior of the layers (represented by the SP layer of BH-2 at 0.75 m depth) shows that r_u approaches 1.

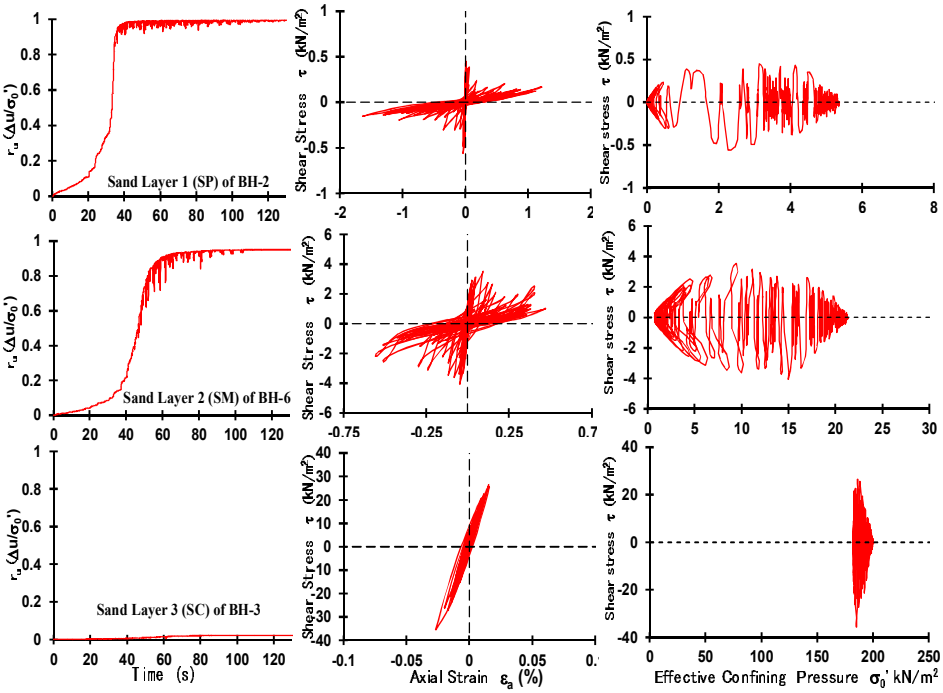

Figure 10 Examples of liquefiable soil behavior at the investigated locations for various sand types.

The hysteresis loop tends to become progressively flatter because of soil elements starting to liquefy. This indicates that there is a reduction of shear modulus (G) during cyclic mobility. After liquefaction, the loop becomes almost horizontal and τ is very close to zero. The cyclic mobility also reduces the effective confining pressure. This indicates that the soil layer loses the τ because σ_v' is reduced by excess pore water pressure. In the SM layers (represented by the SM layer of BH-6 at a depth of 3.75 m), soil behaviors also showed a similar trend as the SP layers. However, $r_u$max still does not reach the liquefaction threshold ($r_u \approx 1$), but is very close to 1 (about 0.948).

The hysteresis loop drops and becomes horizontally flat, but less significantly compared to the SP layers. The existence of higher soil resistance tends to increase the liquefaction strength in this layer, especially for the soils layer at greater depth (larger σ_v'). These layers seem to undergo liquefaction if a stronger earthquake happens. In the SC layers (represented by the SC layer of

BH-8 at 25.5 m depth), $r_u$max was very small (0.022). This indicates that the soil layer is safe from liquefaction during earthquakes. This is also confirmed by the linear hysteresis loop, which indicates that there is no significant degradation of (G) and τ. The earthquake also did not significantly decrease the effective confining pressure, which means the soil layer has sufficient resistance to retain liquefaction.

4.3 Amplification Factor of Liquefiable Layers

Table 2 presents the amplification factor of the soil layers in the investigated sites. In can be seen in Table 2 that the BH-2 site had the highest amplification factor in the investigated area, while BH-1 had the lowest amplification factor. This indicates that BH-2 can possibly undergo serious impact of an earthquake, including liquefaction, which was massively found during the September 2007 earthquake (EERI [10]).

Table 2 Amplification factor of the investigated sites.

Amplification Factor							
BH-1	**BH-2**	**BH-3**	**BH-4**	**BH-5**	**BH-6**	**BH-7**	**BH-8**
1.115	1.480	1.142	1.283	1.134	1.168	1.277	1.339

4.4 FSL and PL AGAINST $r_u$max

The interpretations of FS_L and P_L against $r_u$max are presented in Figure 11. In Figure 11, a larger $r_u$max means a smaller FS_L and a larger $r_u$max tends to increase P_L. The comparison of the results also shows that the plotted points deal with the empirical approach proposed by Yegian and Vittel in [18].

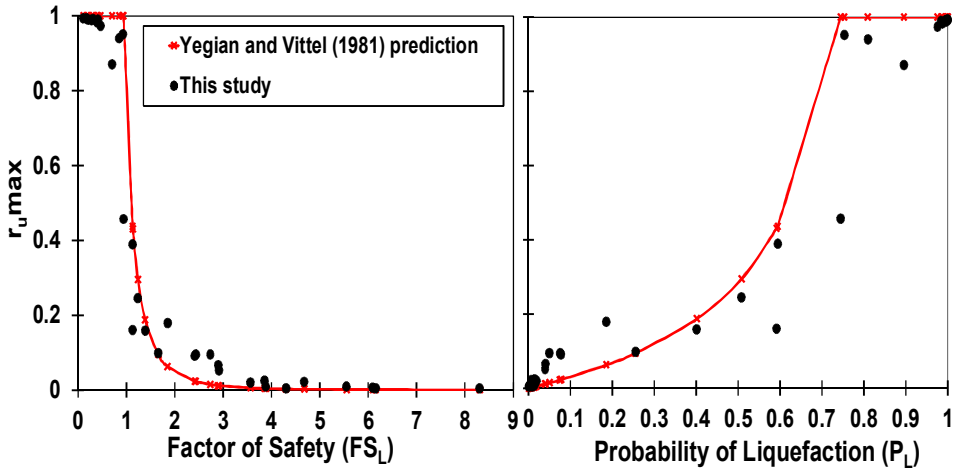

Figure 11 Interpretation of FS_L-P_L and $r_u$max relationships.

5 Conclusion

Liquefaction possibly occurred at shallow depths (0 to 7.5 m) dominated by SP with low soil resistance. All sites underwent amplification due to the earthquake, which is predicted to contribute to soil damage. $r_u$max values linked to empirical analysis were in good agreement with the prediction by Yegian and Vittel [18].

Acknowledgements

The authors would like to thank the Centre of Earthquake Strong Motion Database for the ground motion of the September 2007 earthquake recorded at Sikuai Island, which was used in this study.

References

[1] Konca, A.O., Avouac, J.P., Sladen, A., Meltzner, A.J., Sieh, K., Fang, P., Li, Z., Galetzka, J., Genrich, J., Chlieh, M. & Natawidjaja, D.H., *Partial Rupture of a Locked Patch of the Sumatra Megathrust during the 2007 Earthquake Sequence*, Nature, **456**(7222), pp. 631-635, December. 2008.

[2] Alif, S.M., Meilano, I., Gunawan, E. & Efendi, J., *Evidence of Postseismic Deformation Signal of the 2007 M8.5 Bengkulu Earthquake and the 2012 M8. 6 Indian Ocean Earthquake in Southern Sumatra, Indonesia, based on GPS Data*, Applied Geodesy, **10**(2), pp. 103-108, 2016.

[3] Misiniyati, R., Mawardi, Besperi, Razali, M.R. & Muktadir, R., *Mapping of Liquefaction Potential of Coastal Area Using Cone Penetration Test in Lempuing, Bengkulu City*, Inersia, **5**(2), pp. 1-8, 2013. (Text in Indonesian and abstract in English).

[4] Monalisa, A., *Liquefaction Probability Analysis of Lempuing Bengkulu*, Final project, Civil Engineering, University of Bengkulu, 2014. (Text in Indonesian and abstract in English).

[5] Mase, L.Z, & Sari, A.N., *A Preliminary Evaluation of Liquefaction Potential of Sandy Soil in Lempuing Sub-district (A Coastal Area in Bengkulu City)*, Inersia, **7**(2), pp. 21-25, 2015. Text in Indonesian and abstract in English).

[6] Mase, L.Z. & Somantri, A.K., *Analysis of Liquefaction Potential in Lempuing Sub-district, Bengkulu City Using Critical Maximum Acceleration*, Potensi, **25**(1), pp. 1-11, 2016. (Text in Indonesian and abstract in English).

[7] Mase, L.Z. & Somantri, A.K., *Liquefaction Study Using Shear Wave Velocity (Vs) Data in Coastal Area of Bengkulu City*, Proceeding of Geotechnics National Seminar, Yogyakarta, pp. 81-86, 2016.

[8] Seed, H.B. & Idriss, I.M., *Simplified Procedure for Evaluating Soil Liquefaction Potential*, Soil Mechanics and Foundations Division ASCE, **97**(SM9), pp. 1249-273, 1971.

[9] Idriss, I.M. & Boulanger, R.W., *Semi-empirical Procedures for Evaluating Liquefaction Potential during Earthquakes*, Soil Dynamics and Earthquake Engineering, **26**(1), pp. 115-30, 2006.

[10] Earthquake Engineering Research Institute (EERI), *Learning from Earthquakes Observation on the Southern Sumatra Earthquakes of September 12-13, 2007*, EERI Special Report, Earthquake Engineering Research Institute, California, September 2007.

[11] Ishihara K., Tatsuoka, F. & Yasuda, S., *Undrained Deformation and Liquefaction of and under Cyclic Stresses,* Soils and Foundation, **15**(1), pp. 29-44, 1975.

[12] Elgamal, A., Yang, Z. & Lu, J., *Cyclic1D: a Computer Program for Seismic Ground Response*, Technical Report, TR-No. SSRP-06/05, University of California at San Diego, California, 2015.

[13] Iai, S., Matsunaga, Y, & Kameoka, T., *Strain Space Plasticity Model for Cyclic Mobility*, Soils and Foundations, **32**(2), pp. 1-15, 1992.

[14] Sawada, S., Ozatsumi, O. & Iai, S., *Analysis of Liquefaction Induced Residual Deformation for Two Types of Quay Walls: Analysis by "FLIP"*, 12th World Conference in Earthquake Engineering, January-February 2000.

[15] Iai, S., Matsunaga, Y. & Kameoka, T., *Analysis of Undrained Cyclic Behaviour of Sand under Anisotropic Consolidation*, Soils and Foundations, **32**(2), pp.16-20, 1992.

[16] Liao, S.C., Veneziano, D., & Whitman, R.V., *Regression Models for Evaluating Liquefaction Probability*, Geotechnical Engineering ASCE, **114**(4), pp. 389-410, April. 1988.

[17] Chen, C.J. & Juang, C.H, *Calibration of SPT-CPT based liquefaction Evaluation Methods, Innovations Applications in geotechnical site characterization*, ASCE, **97**(Special Edition), pp. 49–64, 2000.

[18] Yegian, M.K. & Vitteli, B.M., *Analysis of Liquefaction: Empirical Approach*, Proceeding of the 1st International Conference on Recent Advance in Geotechnical Earthquake Engineering and Soil Dynamics, Missouri, April-May 1981.

[19] National Earthquake Hazard Reduction Program (NEHRP), *Recommended Provisions for Seismic Regulation for New Buildings and other Structures 1997 edition*, Technical Report, FEMA 302, Federation Emergency Management Agency, Washington 1998.

[20] Centre of Earthquake Strong Motion Data (CESMD), *Earthquake Data of the 2007 Sumatra Earthquake for Sikulai Island Data*, https://www.strongmotioncenter.org. (Accessed on 13 April 2017)

[21] Youngs, R.R., Chiou, S-J., Silva, W.J. & Humprey, J.R., *Strong Ground Motion Attenuation Relationships for Subduction Zone Earthquakes*, Seismological Research Letter, **68**(1), pp. 58-73, 1997.
[22] Morita, T., Iai, S., Hanlong, L., Ichii, K. & Sato, Y., *Simplified Parameter to Determine Parameter of FLIP*, Technical Report, TR No. 869, Port and Harbour Research Institute, Yokohama, June 1997. (Text in Japanese)